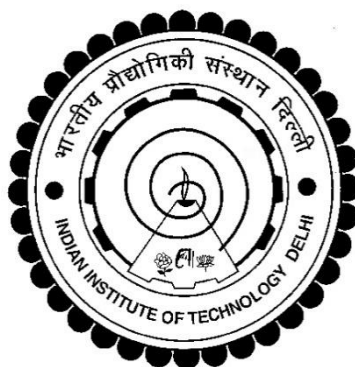


**STRUCTURAL LANDSCAPE OF MANGANESE(II)
AROMATIC DICARBOXYLATE BASED
FUNCTIONALIZED COORDINATION POLYMERS:
SYNTHESIS-STRUCTURE-PROPERTY CORRELATION**

BHARTI SINGH



**DEPARTMENT OF CHEMISTRY
INDIAN INSTITUTE OF TECHNOLOGY DELHI**

AUGUST 2022

© Indian Institute of Technology Delhi (IITD), New Delhi 2022

**STRUCTURAL LANDSCAPE OF MANGANESE(II)
AROMATIC DICARBOXYLATE BASED
FUNCTIONALIZED COORDINATION POLYMERS:
SYNTHESIS-STRUCTURE-PROPERTY CORRELATION**

by

BHARTI SINGH

DEPARTMENT OF CHEMISTRY

Submitted

In fulfillment of the requirements of the degree of Doctor of Philosophy

to the



INDIAN INSTITUTE OF TECHNOLOGY DELHI

AUGUST 2022

Dedicated
To
my family and Teachers

CERTIFICATE

This is to certify that the thesis entitled, “**Structural landscape of manganese(II) aromatic dicarboxylate based functionalized coordination polymers: synthesis-structure-property correlation**” being submitted by **Ms. Bharti Singh** to the Indian Institute of Technology Delhi for the award of the degree of **Doctor of Philosophy** in Chemistry, is a record of bonafide research work carried out by her. Ms. Bharti Singh has worked under my guidance and supervision and has fulfilled the requirements for the submission of this thesis, which to my knowledge has reached the requisite standard.

The results contained in this dissertation have not been submitted, in part or full, to any other university or institute for award of any degree or diploma.

Dr. A. RAMANAN
Professor
Department of Chemistry
Indian Institute of Technology Delhi
New Delhi-110016

ACKNOWLEDGEMENT

*It's a true blessing from God to me to have **Prof. A. Ramanan** as my mentor, supervisor and teacher. He is an epitome of knowledge and wisdom, yet he is very humble and kind-hearted. He is a true visionary. Because of him, lives of countless students have been shaped for the good and I am also one of them. I express my deepest gratitude to sir without his guidance, co-operation and support this thesis would not have taken this shape. He is the one who has given me vision to see the world with multi dimensions. I want to thank him with all my heart.*

I wish to express my sincere thanks to the heads of the Department of Chemistry, Prof. Ravi Shankar, Prof. Anil J. Elias and Prof. N. D. Kurur for their valuable contribution and support throughout my Ph.D work at IIT Delhi. I would also like to thank all the staff associated with the Department of Chemistry, IIT Delhi. I am also thankful to Prof. A. Sundaresan, Chemistry and Physics of Materials Unit, Jawaharlal Nehru Centre for Advanced Scientific Research, Bangalore; Prof. Natasha A. Chernova, Department of Chemistry and Materials Science and Engineering Program, State University of New York, Binghamton, New York; Dr. Ashutosh C Abhyankar and Kaumudi Yadav, Department of Material Engineering, Defence Institute of Advanced Technology, Pune; Prof. Sujit Choudhary, Nanhe Kumar Gupta, Nakul Kumar, Rishabh Shukla and Balwant Singh Chauhan, Department of Physics, Indian Institute of Technology Delhi, New Delhi for magnetic measurements. Discussion with them enabled me to understand the magnetic properties of solids better and this greatly helped me to design the data collection. I would also like to extend my sincere thanks to Swapan. K. Pati and Madhulika Mazumder, Theoretical Sciences Unit, School of Advanced Materials (SAMAT), Jawaharlal Nehru Centre for Advanced Scientific Research, Bangalore for computational studies on magnetic interactions and valuable discussion on the results.

I am highly obliged to Dr. Nicholas Chilton, Department of Chemistry, University of Manchester U.K for his valuable time to make me understand the PHI program to evaluate the exchange parameters.

I would like to thank all my school, graduation and post-graduation teachers for helping me throughout my studies and inspiring me to pursue my career in research.

I would like to convey my heartfelt gratitude to my seniors Dr. Vineet Kumar, Dr. Balendra, Dr. Preethi Thomas, to teach me various techniques and also for becoming a wonderful advisor to ease my path in the whole journey. I would like to thank my colleagues, Shailabh Tewari and Manisha Jadon for creating friendly atmosphere in the lab. I thank my roommate Juhi Chakraborty for being a best roommate and friend. I would also like to thank all my departmental colleagues specially Dr. Archishmati Dubey, Preeti Mishra, Jyoti, Shalini, Shwetambara Jha for being wonderful friends. I have no words to express my thankfulness to all of my friends who have stood by me through all of the ups and downs in my life and continue to do so.

Finally, and most importantly, I want to express my heartfelt gratitude to my family. My mother and father's unconditional love and blessings have shaped who I am today, and I owe everything to them. I am grateful to my sisters and brother-in-law for their constant support and encouragement. My nephew Shivi deserves a special thank you for her puerile support. I consider myself extremely fortunate to have these individuals in my life as a family.

My Ph. D thesis is dedicated to my family and teachers.

Bharti Singh

ABSTRACT

Crystal engineering provides a platform to understand crystal packing of a series of coordination polymers (CPs) employing data mining and retroanalysis. Rationalization of a structural landscape enables one to interpret self-assembly of soluble molecular species condensing into a crystal. Thus, one could design new and functional CPs for various applications providing a path to comprehend the diverse nature of extended metal-ligand architectures. In addition, the tunable and tailorable crystalline structures would become model systems to study synthesis-structure-property with enhanced phenomenological understanding. Crystallization of new CPs from solution is still difficult to predict as the self-assembly processes employed are strongly influenced by subtle variables like solvent, counterion and stoichiometry of the reactants apart from pH and temperature. Among these, solvent molecules could compete for coordination with metal exerting a significant effect on the outcome of the condensed product. Frequently solvent molecules appear as terminal co-ligands in the scaffold which further regulate the formation of the framework during self-assembly. In a few cases, the solvent molecules could occupy pores or empty spaces; these are referred as lattice solvents. Out of numerous applications foreseen for CPs, magnetic properties are of special interest. Synthetic and theoretical chemists have been looking for polynuclear coordination complex based solids containing transition metal ion(s) in intramolecular spin communication as a way to advance new generation of magnetic materials. A major challenge, however, is to effectively control interactions between magnetic centers in the engineered crystal. In this context, manganese carboxylates are ideal candidates as the metal occurs in various oxidation states (+2 to +4 with $S=5/2$ to $3/2$ respectively) and the metal-carboxylate linkages provide diverse frameworks. Manganese(II) compounds in the high spin ground state ($S=5/2$) are particularly important due to the possibility of strong exchange interaction between $3d$ -electrons.

The magnetic centers with varying unpaired electrons provide a variety of magnetic ordering - spin frustrated multiferroics to single molecule magnetism(SMM). Our lab has been employing a crystal engineering approach to crystallize high nuclear manganese clusters in various polar aprotic/protic solvents. One of our objectives is to rationalize the varied coordination assemblies and study the effect of carboxylates on spin-exchange interactions. In this work, we present our approach to the structural design of new manganese carboxylate coordination polymers, as well as the influence of noncovalent interactions, particularly coordination and H-bonding forces on the overall supramolecular assembly and its magnetic behavior in Chapters II-VI and Appendix I.

Chapter I provides a brief account of our literature survey on the crystal engineering of manganese(II) aromatic dicarboxylate based coordination polymers as well as motivation for the present work. Chapter II discusses the crystallization of manganese(II) with the flexible dicarboxylate, benzophenone-4,4'-dicarboxylic acid (*4,4'-H₂bpdC*) under varying solvothermal condition in different aprotic solvents (DMF, DMA and DMSO). The crystal packing of the three isostructural manganese(II) benzophenone-4,4'-dicarboxylate based CPs was greatly influenced through hydrogen bonding exerted by the coordinated solvent molecule (H₂O, DMF or DMSO) occupying the apical position. Low-temperature antiferromagnetic interactions arising in these solids correlate with the variation in the packing of the layers as confirmed by theoretical calculations. Chapter III examines the influence of N-donor based auxiliary ligands in effecting the structural diversity of the system Mn(II)-*4,4'-H₂bpdC*-solvent. The auxiliary ligands, were intended to restrict manganese coordination sites thereby controlling the metal-carboxylate network. Chapter IV addresses how the structural architectures reported in Chapters II and III, vary when a positional isomer of dicarboxylate, such as benzophenone-2,4'-dicarboxylate (*2,4'-bpdC*) is used. Chapter V reports how crystallization is influenced when we reacted methyl substituted

2,2'-*bipy* and *phen* (Chapters III and IV) with the most celebrated rigid ligands, 1,4-benzene dicarboxylic acid (*H₂bdc*) and 2,6-naphthalene dicarboxylic acid (*H₂nda*). Magnetic property of all the manganese dicarboxylates reported in this thesis showed antiferromagnetic interactions at low temperatures. We have made an attempt to correlate magnetic property with crystal structure. Chapter VI discusses nucleation and crystal packing of all crystals reported here in terms of supramolecular assembly of soluble molecules at supersaturation. Our work demonstrates 1:1 manganese aromatic dicarboxylate is the major building block that eventually condenses into a crystal with a defined stoichiometry. Chapter VII provides a brief summary of the results obtained in this study and concludes highlighting future directions.

सार

क्रिस्टल इंजीनियरिंग डेटा माइनिंग और रेट्रोएनालिसिस को नियोजित करने वाले समन्वय पॉलिमर (सीपी) की एक श्रृंखला के क्रिस्टल पैकिंग को समझने के लिए एक मंच प्रदान करता है। एक संरचनात्मक परिदृश्य का युक्तिकरण एक क्रिस्टल में संघनित घुलनशील आणविक प्रजातियों के स्व-संयोजन की व्याख्या करने में सक्षम बनाता है। इस प्रकार, कोई भी विस्तारित धातु-लिगेंड आर्किटेक्चर की विविध प्रकृति को समझने के लिए मार्ग प्रदान करने वाले विभिन्न अनुप्रयोगों के लिए नए और कार्यात्मक सीपी डिजाइन कर सकता है। इसके अलावा, ट्यून करने योग्य और अनुरूप क्रिस्टलीय संरचनाएं संश्लेषण-संरचना-संपत्ति का अध्ययन करने के लिए बड़ी हुई घटना संबंधी समझ के साथ मॉडल सिस्टम बन जाएंगी। समाधान से नए सीपी के क्रिस्टलीकरण की भविष्यवाणी करना अभी भी मुश्किल है क्योंकि नियोजित स्व-संयोजन प्रक्रियाएं पीएच और तापमान के अलावा अभिकारकों के सॉल्वेंट, काउंटरियन और स्टोइकोमेट्री जैसे सूक्ष्म चर से काफी प्रभावित होती हैं। इनमें से, विलायक अणु संघनित उत्पाद के परिणाम पर महत्वपूर्ण प्रभाव डालने वाले धातु के साथ समन्वय के लिए प्रतिस्पर्धा कर सकते हैं। अक्सर विलायक अणु पाइ में टर्मिनल सह-लिगेंड के रूप में दिखाई देते हैं जो स्व-संयोजन के दौरान ढांचे के गठन को और नियंत्रित करते हैं। कुछ मामलों में, विलायक के अणु छिद्रों या रिक्त स्थानों पर कब्जा कर सकते हैं; इन्हें जाली सॉल्वेंट्स के रूप में जाना जाता है। सीपी के लिए अनुमानित कई अनुप्रयोगों में से, चुंबकीय गुण विशेष रुचि के हैं। सिंथेटिक और सैद्धांतिक रसायनज्ञ

नई पीढ़ी की चुंबकीय सामग्री को आगे बढ़ाने के तरीके के रूप में इंटरमोल्युलर स्पिन संचार में संक्रमण धातु आयन (ओं) वाले पॉलीन्यूक्लियर कोऑर्डिनेशन कॉम्प्लेक्स आधारित ठोस की तलाश कर रहे हैं। हालांकि, एक बड़ी चुनौती इंजीनियर क्रिस्टल में चुंबकीय केंद्रों के बीच बातचीत को प्रभावी ढंग से नियंत्रित करना है। इस संदर्भ में, मैंगनीज कार्बोक्सिलेट्स आदर्श उम्मीदवार हैं क्योंकि धातु विभिन्न ऑक्सीकरण अवस्थाओं में होती है (क्रमशः +2 से +4 एस = 5/2 से 3/2 के साथ) और धातु-कार्बोक्सिलेट लिंकेज विविध ढांचे प्रदान करते हैं। 3डी-इलेक्ट्रॉनों के बीच मजबूत विनिमय संपर्क की संभावना के कारण उच्च स्पिन ग्राउंड अवस्था (एस = 5/2) में मैंगनीज (द्वितीय) यौगिक विशेष रूप से महत्वपूर्ण हैं। अलग-अलग अयुग्मित इलेक्ट्रॉनों के साथ चुंबकीय केंद्र विभिन्न प्रकार के चुंबकीय क्रम प्रदान करते हैं - एकल अणु चुंबकत्व (SMM) को स्पिन निराश मल्टीफेरिक्स। हमारी प्रयोगशाला विभिन्न ध्रुवीय एप्रोटिक/प्रोटिक सॉल्वेंट्स में उच्च परमाणु मैंगनीज समूहों को क्रिस्टलीकृत करने के लिए एक क्रिस्टल इंजीनियरिंग दृष्टिकोण को नियोजित कर रही है। हमारा एक उद्देश्य विभिन्न समन्वय संयोजनों को युक्तिसंगत बनाना और स्पिन-एक्सचेंज इंटरैक्शन पर कार्बोक्सिलेट्स के प्रभाव का अध्ययन करना है। इस काम में, हम नए मैंगनीज कार्बोक्सिलेट समन्वय पॉलिमर के संरचनात्मक डिजाइन के साथ-साथ गैर-सहसंयोजक इंटरैक्शन के प्रभाव, विशेष रूप से समग्र सुपरमॉलेक्यूलर असेंबली पर समन्वय और एच-बॉन्डिंग बलों और अध्याय II-VI (परिशिष्ट I) में इसके चुंबकीय व्यवहार के लिए अपना दृष्टिकोण प्रस्तुत करते हैं।

अध्याय I मेंगनीज (II) एरोमैटिक डाइकारबॉक्साइलेट आधारित समन्वय पॉलिमर के क्रिस्टल इंजीनियरिंग के साथ-साथ वर्तमान कार्य के लिए प्रेरणा पर हमारे साहित्य सर्वेक्षण का एक संक्षिप्त विवरण प्रदान करता है। अध्याय II विभिन्न एप्रोटिक सॉल्वेंट्स (डीएमएफ, डीएमए और डीएमएसओ) में अलग-अलग सॉल्वोथर्मल स्थिति के तहत लचीले डाइकारबॉक्साइलेट, बेंजोफेनोन-4,4'-डाइकारबॉक्सिलिक एसिड (4,4'-एच₂बीपीडीसी) के साथ मेंगनीज (II) के क्रिस्टलीकरण पर चर्चा करता है। तीन आइसोस्ट्रक्चरल मेंगनीज (II) बेंजोफेनोन-4,4'-डाइकारबॉक्साइलेट आधारित सीपी की क्रिस्टल पैकिंग, समन्वित सॉल्वेंट अणु (H₂O, DMF या DMSO) द्वारा शीर्ष स्थिति में रहने वाले हाइड्रोजन बॉन्डिंग के माध्यम से बहुत प्रभावित हुई थी। इन ठोस पदार्थों में उत्पन्न होने वाले निम्न-तापमान एंटीफेरोमैग्नेटिक इंटरैक्शन सैद्धांतिक गणनाओं द्वारा पुष्टि की गई परतों की पैकिंग में भिन्नता के साथ सहसंबद्ध होते हैं। अध्याय III प्रणाली Mn(II)-4,4'-H₂bpdC-विलायक की संरचनात्मक विविधता को प्रभावित करने में N-दाता आधारित सहायक लिगेंड के प्रभाव की जांच करता है। सहायक लिगेंड्स का उद्देश्य मेंगनीज समन्वय साइटों को प्रतिबंधित करना था जिससे धातु-कार्बोक्सिलेट नेटवर्क को नियंत्रित किया जा सके। अध्याय IV यह बताता है कि अध्याय II और III में रिपोर्ट की गई संरचनात्मक संरचनाएँ कैसे भिन्न होती हैं, जब डाइकारबॉक्साइलेट के एक स्थितीय समावयव, जैसे कि बेंजोफेनोन-2,4'-डाइकारबॉक्साइलेट (2,4'-bpdC) का उपयोग किया जाता है। अध्याय V रिपोर्ट करता है कि जब हमने सबसे प्रसिद्ध कठोर लिगेंड्स, 1,4-बेंजीन डाइकारबॉक्सिलिक एसिड (H₂bdc) और 2,6-नेफथलीन डाइकारबॉक्सिलिक के साथ मिथाइल प्रतिस्थापित 2,2'-bipy और फेन (अध्याय III और

IV) पर प्रतिक्रिया की तो क्रिस्टलीकरण कैसे प्रभावित होता है। एसिड (H₂nda)। इस थीसिस में बताए गए सभी मैंगनीज डाइकार्बोक्साइलेट्स की चुंबकीय संपत्ति ने कम तापमान पर एंटीफेरोमैग्नेटिक इंटरैक्शन दिखाया। हमने चुंबकीय गुण को क्रिस्टल संरचना के साथ सहसंबंधित करने का प्रयास किया है। अध्याय VI सुपरसैचुरेशन पर घुलनशील अणुओं की सुपरमॉलेक्यूलर असेंबली के संदर्भ में यहां बताए गए सभी क्रिस्टल के न्यूक्लियेशन और क्रिस्टल पैकिंग पर चर्चा करता है। हमारे काम से पता चलता है कि 1: 1 मैंगनीज एरोमैटिक डाइकार्बोक्साइलेट प्रमुख बिल्डिंग ब्लॉक है जो अंततः एक परिभाषित स्टोइकोमेट्री के साथ एक क्रिस्टल में संघनित होता है। अध्याय VII इस अध्ययन में प्राप्त परिणामों का एक संक्षिप्त सारांश प्रदान करता है और भविष्य की दिशाओं पर प्रकाश डालते हुए निष्कर्ष निकालता है।

TABLE OF CONTENTS

CERTIFICATE.....	i
ACKNOWLEDGEMENTS.....	ii
ABSTRACT.....	iv
LIST OF CONTENT.....	xi
LIST OF FIGURES.....	xv
LIST OF TABLES.....	xxiv
LIST OF SCHEMES.....	xxvii
ABBREVIATIONS.....	xxix

LIST OF CONTENT

Chapter I

Introduction

I.1 Introduction.....	2
I.2 Crystal engineering.....	3
I.3 Coordination polymers - An emerging class of crystalline materials.....	4
I.4 Classification of coordination polymers (CPs).....	5
I.5 Cambridge Structural Database (CSD).....	9
I.6 Magnetic coordination polymers: An emerging class of materials.....	11
I.6.1 Magneto-structural correlations among simple manganese salts- chloride, hydroxide, sulphate, formate, acetate and oxalate.....	11

I.6.2 Magnetic properties of solids and its characterization	18
I.7 Motivation for the present work.....	21
References.....	31

Chapter II

Structural diversity of system, manganese(II) salt-benzophenone-4,4'-dicarboxylic acid-solvent

II.1 Introduction.....	44
II.2 Experimental section	46
II.2.1 High-through put screening studies.....	46
II.2.2 Physical measurements	52
II.2.3 X-ray crystallographic studies.....	53
II.2.4 Computational methods.....	55
II.3 Results and Discussion.....	56
II.3.1 Crystal structures of the solids MnCP1-MnCP3	56
II.3.2 Thermal analysis.....	63
II.3.3 Magnetic properties and Computational studies.....	65
II.4 Summary.....	72
References.....	73

Chapter III

Effect of N-donor based auxiliary ligand on the structural diversity of benzophenone-4,4'-dicarboxylic acid

III.1 Introduction.....	80
III.2 Experimental section	81

III.2.1 High-through put screening studies.....	82
III.2.2 Physical measurements	92
III.3 Results and Discussion.....	95
III.3.1 Crystal structures of the solids MnCP4-MnCP10.....	95
III.3.2 Magnetic behavior of the solids.....	109
III.3.3 Thermal analysis.....	113
III.4 Summary.....	116
References.....	117
Chapter IV	
Structural diversity of benzophenone-2,4'-dicarboxylic acid	
IV.1 Introduction.....	121
IV.2 Cambridge structural database (CSD) Survey.....	122
IV.3 Experimental section	122
IV.3.1 High-through put screening studies.....	123
IV.3.2 Physical measurements	133
IV.4 Results and Discussion.....	136
IV.4.1 Crystal structures of the solids MnCP11-MnCP16.....	136
IV.4.2 Structural chemistry of <i>4,4'-H₂bpdc</i> and <i>2,4'-H₂bpdc</i>	150
IV.4.3 Thermal analysis	151
IV.4.4 Magnetic behavior of the solids	153
IV.5 Summary.....	159
References.....	160

Chapter V

Effect of substituents of N-donor based auxiliary ligands on framework with rigid dicarboxylate ligands

V.1 Introduction.....	164
V.2 CSD analysis.....	165
V.3 Experimental section	165
V.3.1 High-through put screening studies.....	166
V.3.2 Physical measurements	179
V.4 Results and Discussion.....	184
V.4.1 Crystal structures of the solids MnCP17-MnCP25.....	184
V.4.2 Thermal analysis	205
V.4.3 Magnetic behavior of the solids	206
V.5 Summary.....	215
References.....	216

Chapter VI

Perspective on crystallization of manganese(II) aromatic dicarboxylate based coordination polymers-Understanding crystal packing in terms of supramolecular aggregation

VI.1 Introduction.....	220
VI.1.1 Structural landscape of the system, MnCl ₂ -H ₂ O.....	222
VI.1.2 Structural landscape of the system, MnSO ₄ -H ₂ O.....	224
VI.1.3 Structural landscape of the system, Mn(HCOO) ₂ -H ₂ O.....	227

VI.1.4 Structural landscape of the system, Mn(OAc) ₂ -H ₂ O.....	229
VI.2 Crystallization of manganese(II)-4,4'- <i>bpdc</i> coordination polymers (refer Chapter II).....	231
VI.3 Structural landscape of manganese(II)-4,4'- <i>bpdc</i> coordination polymers (refer Chapter III).....	234
VI.4 Structural landscape of manganese(II)-2,4'- <i>bpdc</i> coordination polymers (refer Chapter IV).....	239
VI.5 Structural landscape of the system manganese(II)- rigid aromatic dicarboxylic acid-auxiliary ligand-solvent (refer Chapter V).....	244
VI.6 Summary.....	250
References.....	251

Chapter VII

Summary, Conclusions and Future directions.....	252-256
---	---------

APPENDIX I

Hyperlink for crystallographic information files (CIFs) of solids MnCP1-MnCP25.....	257
Rietveld refinement of PXRD pattern of solids MnCP1-MnCP25	257

APPENDIX II

FT-Infrared Spectra of solids MnCP1 – MnCP25.....	263
---	-----

APPENDIX III

Magnetic behavior of system, Mn(II)- 4,4'-sulphonyldibenzoic acid(<i>H₂SBA</i>)-auxiliary ligand-solvent.....	272
--	-----

ACADEMIC RESUME OF AUTHOR	283-285
--	---------

LIST OF FIGURES

Figure I.1. Dimensionality of coordination polymers - 1D (chain), 2D (sheet) and 3D through metal-carboxylate coordination linkage. Crystal packing of chains or sheets are through H-bonding and other weak noncovalent interactions.....	6
---	---

Figure I.2 Salient features of coordination polymers (CPs).....	7
--	---

Figure I.3 Different pathways employed for crystallization of multicomponent metal-organic solids.....	8
Figure I.4 Growth of CSD and MOF entries since 1972 - report from CCDC website.....	9
Figure I.5 Applications of coordination polymers/ metal-organic frameworks.....	10
Figure I.6 Different bridging modes of dicarboxylate linkers.....	14
Figure I.7 Structural assembly of the cluster, $[\text{Mn}^{\text{III,IV}}_{12}\text{O}_{12}(\text{CH}_3\text{COO})_{16}(\text{H}_2\text{O})_4]$. The four Mn^{4+} and eight Mn^{3+} ions in octahedral coordination are bridged through acetate and oxo groups for a neutral molecular cluster. $\{\text{Mn}^{\text{IV}}(\text{CH}_3\text{COO})_{1/2}\text{O}_{5/3}\}_4\{\text{Mn}^{\text{III}}(\text{CH}_3\text{COO})_{4/2}\text{O}_{2/3}\}_4$ $\{\text{Mn}^{\text{III}}(\text{CH}_3\text{COO})_{3/2}\text{O}_{2/3}(\text{H}_2\text{O})_{1/1}\}_4 \equiv [\text{Mn}^{\text{IV}}_4\text{Mn}^{\text{III}}_8\text{O}_{12}(\text{CH}_3\text{COO})_{16}(\text{H}_2\text{O})_4]$	16
Figure I.8 Pictorial representation of spin alignments in ferro-, antiferro-, ferri- and canted antiferromagnetic materials.....	19
Figure I.9 Representation of Curie-Weiss law and magnetic phase transitions.....	20
Figure I.10 A comparative representation of the number of manganese-based CPs reported (source: CSD version 5.43 and Scifinder).....	21
Figure II.1 (a) Coordination environment of Mn(II) in MnCP1. (b) A pair of distorted square pyramidal $\{\text{MnO}_5\}$ are bridged by the carboxylate group of <i>4,4'</i> - <i>bpdc</i> forming 1D chains.....	57
Figure II.2 (a) The zig-zag sheet on the bc-plane in MnCP1 viewed along a-axis. (b) Distorted square pyramidal polyhedron $\{\text{MnO}_5\}$ bridged by the carboxylates group of <i>4,4'</i> - <i>bpdc</i> forming a 2D coordination network on ac-plane. Hydrogens are omitted from <i>4,4'</i> - <i>bpdc</i> for clarity.....	58
Figure II.3 The supramolecular architecture of MnCP1 viewed along a-axis. A strong O–H···O interaction (shown in yellow region) between the coordinated H ₂ O on one sheet and the carboxylate groups from adjacent sheets led to zig-zag layers.....	58
Figure II.4 (a) Coordination environment of Mn(II) in MnCP2. (b) Distorted manganese octahedra $\{\text{MnO}_6\}$ are bridged by the carboxylate groups of <i>4,4'</i> - <i>bpdc</i> forming chains.....	59
Figure II.5 (a) 2D sheet in MnCP2 viewed along c-axis. (b) Distorted manganese octahedra bridged by the carboxylates groups of <i>4,4'</i> - <i>bpdc</i> forming 2D coordination network on ac-plane. Hydrogens of <i>4,4'</i> - <i>bpdc</i> are omitted for clarity.....	60
Figure II.6 The supramolecular architecture of MnCP2 viewed along the c-axis. A weaker C–H···O interaction (shown in yellow region) between the coordinated DMF on one sheet and the	

carboxylate group from the adjacent sheet. Unlike MnCP1, the stacking of the sheets in MnCP2 are almost parallel. Hydrogens of the ligand are omitted for clarity.....61

Figure II.7 (a) Coordination environment of Mn in MnCP3. (b) Distorted manganese octahedra bridged by the carboxylate groups of *4,4'*-*bpdc* forming chains.....62

Figure II.8 (a) 2D sheet of MnCP3 viewed along the *a*-axis. (b) Distorted {MnO₆} bridged by the carboxylates group of *4,4'*-*bpdc* forming a 2D network on *ac*-plane.....62

Figure II.9 The supramolecular architecture of MnCP3 viewed along *c*-axis. A comparatively stronger C–H···O interaction (shown in yellow region) between DMSO on one sheet and the carboxylate group from the adjacent sheet. Unlike MnCP1, the stacking of the sheets in MnCP3 are almost parallel like in MnCP2. Hydrogens of the ligand are omitted for clarity.....63

Figure II.10 TGA curves for solids MnCP1-MnCP3.....64

Figure II.11 Temperature Dependence of the $\chi_M T$ product in the temperature range 2-300K at 0.1 T of solid MnCP1-MnCP3. Temperature dependence of χ_M^{-1} representing Curie-Weiss law (orange)*, due to presence of paramagnetic oxygen..... 67

Figure II.12 Mn···Mn contact distances and –Mn–O–Mn– angles in MnCP1-MnCP3..... 67

Figure II.13 Spin Polarized DOS for FM and AFM phases of the three solids.....70

Figure II.14 Isosurfaces showing 3D spin density ($\rho_{\uparrow} - \rho_{\downarrow}$) with the isosurface at $0.5 \times 10^{-3} e/\text{\AA}^3$ on Mn atoms for a) MnCP1, b) MnCP2 and c) MnCP3 systems.....71

Figure II.15 Field-dependent magnetization in the range of ± 7 T at 2 and 300K.....71

Figure III.1 Distorted octahedral {MnO₄N₂} polyhedrons bridged by the carboxylate group of *4,4'*-*bpdc* forming a dimer.....98

Figure III.2 Distorted octahedra polyhedrons {MnO₄N₂} are bridged by the carboxylates group of *4,4'*-*bpdc* forming a 1 D chain. Hydrogens are omitted from *4,4'*-*bpdc* for clarity.....98

Figure III.3 A strong O–H···O interaction (shown in yellow region - O···O, 2.714 Å) between the coordinated H₂O on one chain and the carboxylate group from adjacent chain led to 3D architecture.....99

Figure III.4 Distorted octahedral polyhedrons bridged by the carboxylate groups of *4,4'*-*bpdc* forming a corner-shared trimer.....100

Figure III. 5 Distorted octahedra polyhedrons {MnO₄N₂} are bridged by carboxylate groups of *4,4'*-*bpdc* forming 1D chain. Hydrogens are omitted from *4,4'*-*bpdc* for clarity.....101

Figure III.6 Distorted octahedral polyhedrons bridged by the carboxylate group of *4,4'*-*bpdc* forming a corner shared trimer.....102

Figure III.7 Distorted octahedra polyhedrons $\{\text{Mn}_3\text{O}_{12}\text{N}_4\}$ are bridged by the carboxylates group of <i>4,4'-bpdc</i> forming a 3D architecture. Hydrogens are omitted from <i>4,4'-bpdc</i> for clarity.....	103
Figure III.8 Distorted octahedrons $\{\text{MnN}_2\text{O}_4\}$ are bridged by the <i>4,4'-bpdc</i> to form anionic one-dimensional chain along <i>c</i> -axis. This anionic charge on the manganese carboxylate chain is balanced by the cationic moiety. Hydrogens are omitted from <i>4,4'-bpdc</i> for clarity.....	104
Figure III.9 (a) A strong O–H···O interaction (shown in yellow region) between the lattice H ₂ O and the carboxylate groups from 1D chain. (b) One dimensional chains are further stabilized by the O–H···O interaction between the coordinated H ₂ O of cationic moiety $[\text{Mn}(5,5'\text{-dimethyl-}2,2'\text{-bipy})(\text{H}_2\text{O})_4]^{2+}$ and carboxylate of <i>4,4'-bpdc</i> , which in turn result into 3D supramolecular architecture.....	105
Figure III.10 Distorted octahedral polyhedrons bridged by the carboxylate group of <i>4,4'-bpdc</i> ligand forming a dimer.....	107
Figure III.11 One dimensional metal dicarboxylates chains are pillared by the <i>4,4'-bipy</i> to form 2D sheets. Lattice DMA solvents are bounded to carbonyl oxygen of <i>4,4'-bpdc</i> of 2D sheet through C–H···O interaction.....	108
Figure III.12 A strong C–H···O(carbonyl) interaction (shown in yellow region) between the carbonyl group on <i>4,4'-bpdc</i> of one sheet and the phenyl group from adjacent sheet led to 3D architecture.....	108
Figure III.13 (a) $\chi_{\text{M}}T$ versus T plot and (b) χ_{M} versus T in the range 5-300K at 0.1 T for MnCP4. Fitted Curie-Weiss region is highlighted in orange. (c) Simulated pattern of magnetic susceptibilities versus temperature obtained by PHI program.....	109
Figure III.14 (a) $\chi_{\text{M}}T$ versus T plot and (b) χ_{M} versus T in the range 5-300K at 0.1 T for MnCP5. Fitted Curie-Weiss region is highlighted in orange. (c) Simulated pattern of magnetic susceptibilities versus temperature obtained by PHI program.....	110
Figure III.15 (a) $\chi_{\text{M}}T$ versus T plot and (b) χ_{M} versus T in the range 5-300K at 0.1 T for MnCP8. Fitted Curie-Weiss region is highlighted in orange. (c) Simulated pattern of magnetic susceptibilities versus temperature obtained by PHI program.....	111
Figure III.16 (a) $\chi_{\text{M}}T$ versus T plot and (b) χ_{M} versus T in the range 5-300K at 0.1 T for MnCP10. Fitted Curie-Weiss region is highlighted in orange. (c) Simulated pattern of magnetic susceptibilities versus temperature obtained by PHI program.....	112
Figure III.17 Mn···Mn contact distances and –Mn–O–Mn– angles in solids.....	112
Figure III.18 Field-dependent magnetization in the range of ± 6 T at 5 and 300K.....	113
Figure III.19 TGA curves for solids:(a) MnCP4; (b) MnCP5 (green curve), MnCP6 (pink curve), MnCP7(blue curve); (c)MnCP8; (d)MnCP9; (e)MnCP10.....	114

Figure IV.1 A comparative representation of the coordination environment of dimeric and trimeric manganese(II) dicarboxylates in solids MnCP11-MnCP16.....	136
Figure IV.2 The distorted square pyramidal polyhedrons, {MnO ₅ } are extended into 1D chain along [100] through 2,4'- <i>bpd</i> c. Hydrogens are omitted from the ligand for clarity.....	139
Figure IV.3 (a) The 1D chains interact through C–H··O between the coordinated DMA and the carboxylate group of the adjacent chains. (b) Disordered lattice water interacts with carboxylate oxygen via O··H–Ow. Hydrogens are omitted in some parts for clarity.....	140
Figure IV.4 The dimers are extended by 2,4'- <i>bpd</i> c forming a 1D chain. Hydrogens are omitted from the ligand for clarity.....	141
Figure IV.5 The adjacent chains are stabilized through C–H··O between the phenanthroline benzyl ring and the carbonyl oxygen of 2,4'- <i>bpd</i> c.....	142
Figure IV.6 The trimers {Mn ₃ O ₁₄ N ₂ } are bridged by the carboxylates group of 2,4'- <i>bpd</i> c ligand forming a 2D sheet on <i>ab</i> -plane. Hydrogens are omitted from 2,4'- <i>bpd</i> c ligand for clarity.....	143
Figure IV.7 The sheets are further stabilised through C–H··O between DMA and the carbonyl oxygen of 2,4'- <i>bpd</i> c.....	144
Figure IV.8 The trimeric units, {Mn ₃ O ₁₂ N ₄ } are connected to each other through bridging carboxylates of 2,4'- <i>bpd</i> c to form a 1D chain on <i>ac</i> -plane. Hydrogens are omitted from 2,4'- <i>bpd</i> c for clarity.....	145
Figure IV.9 The 1D chains are further stabilised by C–H··O between the formate from one chain and the phenyl ring of 2,4'- <i>bpd</i> c from the adjacent chain.....	146
Figure IV.10 Trimers {Mn ₃ O ₁₂ N ₄ } are bridged by the carboxylates group of 2,4'- <i>bpd</i> c to form a 2D sheet on <i>ab</i> -plane. Hydrogens are omitted from 2,4'- <i>bpd</i> c for clarity.....	147
Figure IV.11 These chains are supramolecularly assembled by the nonbonding interaction between the methyl group of 4, 4'- <i>dimethyl-2,2'-bipy</i> and carbonyl oxygen of 2,4'- <i>bpd</i> c of the parallel sheet. Hydrogens are omitted from 2,4'- <i>bpd</i> c for clarity.....	148
Figure IV.12 The trimeric unit, {Mn ₃ O ₈ N ₄ Cl ₂ } are extended into 1D chain by 2,4'- <i>bpd</i> c on <i>ac</i> -plane. Hydrogens are omitted from 2,4'- <i>bpd</i> c for clarity.....	149
Figure IV.13 These chains are supramolecularly assembled by the hydrogen bond between the phenyl group of auxillary ligands and the carboxylates group of 2,4'- <i>bpd</i> c of the parallel chain.....	150
Figure IV.14 Comparative structural features of 4,4'- <i>H₂bpd</i> c and 2,4'- <i>H₂bpd</i> c.....	150
Figure IV.15 Thermal analysis of the solids MnCP11-MnCP16.....	152

Figure IV.16 (a) $\chi_M T$ versus T plot and (b) χ_M versus T in the range 2-300K at 0.1 T for MnCP11. Fitted Curie-Weiss region is highlighted in orange. (c) Simulated pattern of magnetic susceptibilities versus temperature obtained by PHI program.....	154
Figure IV.17 (a) $\chi_M T$ versus T plot and (b) χ_M versus T in the range 2-300K at 0.1 T for MnCP12. Fitted Curie-Weiss region is highlighted in orange. (c) Simulated magnetic susceptibilities pattern obtained by PHI program.....	155
Figure IV.18 (a) $\chi_M T$ versus T plot and (b) χ_M versus T in the range 2-300K at 0.1 T for MnCP13. Fitted Curie-Weiss region is highlighted in orange. (c) Simulated magnetic susceptibilities pattern obtained by PHI program.....	156
Figure IV.19 (a) $\chi_M T$ versus T plot and (b) χ_M versus T in the range 2-300K at 0.1 T for MnCP14. Fitted Curie-Weiss region is highlighted in orange. (c) Simulated magnetic susceptibilities pattern obtained by PHI program.....	156
Figure IV.20 (a) $\chi_M T$ versus T plot and (b) χ_M versus T in the range 2-300K at 0.1 T for MnCP16. Fitted Curie-Weiss region is highlighted in orange. (c) Simulated magnetic susceptibilities pattern obtained by PHI program.....	157
Figure V.1 Distorted octahedral $\{Mn_3O_{13}N_2\}$ polyhedrons bridged by the carboxylate group of <i>bdc</i> forming a trimer.....	188
Figure V.2 Distorted octahedra polyhedrons $\{Mn_3O_{13}N_2\}$ are bridged by the carboxylates group of <i>bdc</i> forming a 1D chain. Hydrogens are omitted from <i>bdc</i> for clarity.....	188
Figure V.3 Distorted octahedra polyhedrons $\{Mn_3O_{13}N_2\}$ are bridged by the carboxylates group of <i>bdc</i> forming a 2D sheets. Hydrogens are omitted from <i>bdc</i> for clarity.....	189
Figure V.4 Distorted octahedral $\{Mn_3O_{12}N_4\}$ polyhedrons bridged by the carboxylate group of <i>bdc</i> forming a trimer.....	190
Figure V.5 Distorted octahedra polyhedrons $\{Mn_3O_{12}N_4\}$ are bridged by the carboxylates group of <i>bdc</i> forming a 2D sheets. Hydrogens are omitted from <i>bdc</i> for clarity.....	191
Figure V.6 Distorted octahedral $\{Mn_3O_{12}N_4\}$ polyhedrons bridged by the carboxylate group of <i>bdc</i> forming a trimer.....	192
Figure V.7 Distorted octahedra polyhedrons $\{Mn_3O_{12}N_4\}$ are bridged by the carboxylates group of <i>bdc</i> forming a 2D sheets. Hydrogens are omitted from <i>bdc</i> for clarity.....	193

Figure V.8 Distorted octahedral $\{\text{MnO}_4\text{N}_2\}$ polyhedrons bridged by the carboxylate group of <i>bdc</i> to form 1D zig-zag chain extend along <i>b</i> -axis.....	194
Figure V.9 These chains are supramolecularly assembled by the O–H···O interaction between the coordinated water molecule and carboxylate group of parallel chain.....	194
Figure V.10 Distorted octahedral $\{\text{Mn}_3\text{O}_{12}\text{N}_4\}$ polyhedrons bridged by the carboxylate group of <i>bdc</i> forming a trimer.....	195
Figure V.11 Distorted octahedra polyhedrons $\{\text{Mn}_3\text{O}_{12}\text{N}_4\}$ are bridged by the carboxylates group of <i>bdc</i> forming a 2D sheets. Hydrogens are omitted from <i>bdc</i> for clarity.....	196
Figure V.12 Distorted octahedral $\{\text{Mn}_3\text{O}_{12}\text{N}_4\}$ polyhedrons bridged by the carboxylate group of <i>nda</i> forming a trimer.....	197
Figure V.13 Distorted octahedra polyhedrons $\{\text{Mn}_3\text{O}_{12}\text{N}_4\}$ are bridged by the carboxylates group of <i>nda</i> forming a 3D architecture. Hydrogens are omitted from <i>nda</i> for clarity.....	198
Figure V.14 Distorted octahedral $\{\text{Mn}_2\text{O}_4\text{N}_4\text{Cl}_2\}$ polyhedrons bridged by chloride ions forming a dimer.....	199
Figure V.15 Dimeric $\{\text{Mn}_2\text{O}_4\text{N}_4\text{Cl}_2\}$ units are bridged by the carboxylates group of <i>nda</i> forming a 1D chain. Hydrogens are omitted from <i>nda</i> for clarity.....	200
Figure V.16 These chains are supramolecularly assembled in 3D space via C–H···Cl and C–H···O interactions between adjacent chains.....	200
Figure V.17 Distorted octahedral $\{\text{Mn}_3\text{O}_6\text{N}_4\text{Cl}_4\}$ polyhedrons bridged by the carboxylate group of <i>nda</i> forming a trimer.....	202
Figure V.18 Trimeric $\{\text{Mn}_3\text{O}_6\text{N}_4\text{Cl}_4\}$ units are bridged by the carboxylates group of <i>nda</i> and chloride to form 2D Sheets. Hydrogens are omitted from <i>nda</i> for clarity.....	202
Figure V.19 These 2D sheets are further assembled in 3D space through C–H···Cl interaction between the phenyl ring of auxiliary ligand and chloride group of the adjacent sheets.....	203
Figure V.20 Distorted octahedral $\{\text{Mn}_2\text{O}_{10}\text{N}_2\}$ polyhedrons bridged by the carboxylate group of <i>nda</i> forming a dimer.....	205
Figure V.21 Dimeric $\{\text{Mn}_2\text{O}_{10}\text{N}_2\}$ units are bridged by the carboxylates group of <i>nda</i> forming a 2D architecture. Hydrogens are omitted from <i>nda</i> for clarity.....	205
Figure V.22 Thermal analysis of solids MnCP17-MnCP25.....	205
Figure V.23 (a) $\chi_M T$ versus T plot and (b) $1/\chi_M$ versus T in the range 5-300K at 0.1 T for MnCP17. Fitted Curie-Weiss region is highlighted in orange. (c) Simulated magnetic susceptibilities pattern obtained by PHI program.....	207

Figure V.24 (a) $\chi_M T$ versus T plot and (b) $1/\chi_M$ versus T in the range 5-300K at 0.1 T for MnCP19. Fitted Curie-Weiss region is highlighted in orange. (c) Simulated magnetic susceptibilities pattern obtained by PHI program.....	208
Figure V.25 (a) $\chi_M T$ versus T plot and (b) $1/\chi_M$ versus T in the range 5-300K at 0.1 T for MnCP21. Fitted Curie-Weiss region is highlighted in orange. (c) Simulated magnetic susceptibilities pattern obtained by PHI program.....	208
Figure V.26 (a) $\chi_M T$ versus T plot and (b) $1/\chi_M$ versus T in the range 5-300K at 0.1 T for MnCP22. Fitted Curie-Weiss region is highlighted in orange. (c) Simulated magnetic susceptibilities pattern obtained by PHI program.....	209
Figure V.27 (a) $\chi_M T$ versus T plot and (b) $1/\chi_M$ versus T in the range 5-300K at 0.1 T for MnCP23. Fitted Curie-Weiss region is highlighted in orange. (c) Simulated magnetic susceptibilities pattern obtained by PHI program.....	209
Figure V.28 (a) $\chi_M T$ versus T plot and (b) $1/\chi_M$ versus T in the range 5-300K at 0.1 T for MnCP24. Fitted Curie-Weiss region is highlighted in orange. (c) Simulated magnetic susceptibilities pattern obtained by PHI program.....	210
Figure V.29 Field-dependent magnetization in the range of ± 7 T was measured at 5K.....	211
Figure V.30 Field-dependent magnetization in the range of ± 7 T was measured at 300K.....	211
Figure VI.1 A picture representing nucleation and growth of crystal from a supersaturated solution. The building blocks(tectons) are chemically reasonable soluble metal complexes that are neutral (point zero charge species - PZC) or/and ion-pairs. Crystal nucleus or the supramolecular transition state(TS1 and TS2) represents supramolecular assembly (a liquid-like state) before condensing into a periodic solid.....	221
Figure VI.2 (a) The discrete molecule, $\text{cis-}\{\text{Mn}(\text{H}_2\text{O})_{4/1}\text{Cl}_{2/1}\}$ extended through three-dimensional H-bonded network leading to formation of $\text{MnCl}_2 \cdot 4\text{H}_2\text{O}$ (0D, molecular solid). (b) Noncovalent interaction ($\text{Mn-OH}_2 \cdots \text{Cl}$) between coordinated water and chloride group of adjacent $\{\text{Mn}(\text{H}_2\text{O})_{4/1}\text{Cl}_{2/1}\}$. These tectons are topotactically dehydrated to form $\text{MnCl}_2 \cdot 2\text{H}_2\text{O}$. (c) 1D chains of $\text{MnCl}_2 \cdot 2\text{H}_2\text{O}$ are further stabilized by H-bonded interaction between the coordinated water and chloride of adjacent chains. (d) Crystal structure of 1D chain of $\{\text{Mn}(\text{H}_2\text{O})_{2/1}\text{Cl}_{4/2}\} \equiv \text{MnCl}_2 \cdot 2\text{H}_2\text{O}$	223
Figure VI.3 (a) Crystal structure of 1D $\text{MnCl}_2 \cdot 2\text{H}_2\text{O}$ (b) 1D chains of $\text{MnCl}_2 \cdot 2\text{H}_2\text{O}$ are stabilized by noncovalent interaction ($\text{Mn-OH} \cdots \text{Cl}$) between the coordinated water and chloride group of adjacent chains. (c) These chains are topotactically dehydrated to form to anhydrous MnCl_2 (d) Crystal structure of 2D sheet of $\{\text{MnCl}_{6/3}\} \equiv \text{MnCl}_2$. The sheets are packed through weak $\text{Cl} \cdots \text{Cl}$ interactions.....	223
Figure VI.4 The 1:1 complex, $\{\text{Mn}(\text{H}_2\text{O})_5(\text{SO}_4)\}$ supramolecularly condense to form 3D extended structure through $-\text{Mn}-\text{SO}_4-\text{Mn}-$. The overall composition is $\{\text{Mn}(\text{SO}_4)_{6/4}\} \equiv [\text{Mn}(\text{SO}_4)_2]$	225

- Figure VI.5** The PZC, $\{\text{Mn}(\text{H}_2\text{O})_5(\text{SO}_4)\}$ supramolecularly condense to form extended H-bonded networks. The overall composition is $\{\text{Mn}(\text{H}_2\text{O})_{2/2}(\text{SO}_4)_{4/4}\} \equiv [\text{Mn}(\text{H}_2\text{O})(\text{SO}_4)]$ 226
- Figure VI.6** The PZC specie, $\{\text{Mn}(\text{H}_2\text{O})_5(\text{SO}_4)\}$ supramolecularly condense to form a dimeric unit; the dimer extends through H-bonding interaction $\{\text{H}_2\text{O}\cdots\text{SO}_4\}$ The overall composition is $\{\text{Mn}(\text{H}_2\text{O})_{4/1}(\text{SO}_4)_{2/2}\} \equiv [\text{Mn}(\text{H}_2\text{O})_4(\text{SO}_4)]$ 226
- Figure VI.7** The PZC specie, $\{\text{Mn}(\text{H}_2\text{O})_5(\text{SO}_4)\}$ supramolecularly condense to form a 1D chain. The overall composition is $\{\text{Mn}(\text{H}_2\text{O})_{4/1}(\text{SO}_4)_{1/1}\} \equiv [\text{Mn}(\text{H}_2\text{O})_4(\text{SO}_4)]$. H_2O or $\text{MnSO}_4 \cdot 5\text{H}_2\text{O}$ 227
- Figure VI.8** The PZC specie, $\{\text{Mn}(\text{HCOO})_2(\text{sol})_4\}$ supramolecularly condense to form 3D structure. The overall composition is $\{\text{Mn1}(\text{HCOO})_{6/2}\}\{\text{Mn2}(\text{HCOO})_{2/2}(\text{H}_2\text{O})_{4/1}\} \equiv [\text{Mn}(\text{HCOO})_2(\text{H}_2\text{O})_2]$ 228
- Figure VI.9** The PZC specie, $\{\text{Mn}(\text{HCOO})_2(\text{sol})_4\}$ supramolecularly condense to form 3D structure. The overall composition is $\{\text{Mn}(\text{HCOO})_{6/3}\} \equiv [\text{Mn}(\text{HCOO})_2]$ 228
- Figure VI.10** The PZC specie, $\{\text{Mn}(\text{CH}_3\text{COO})_2(\text{sol})_4\}$ condense to form dimeric unit which extended into the 2D sheet. The overall composition is $\{\text{Mn1}(\text{CH}_3\text{COO})_{4/2}(\text{CH}_3\text{COO}')_{2/3}\}\{\text{Mn2}(\text{CH}_3\text{COO})_{2/2}(\text{CH}_3\text{COO}')_{2/3}(\text{H}_2\text{O})_{2/1}\}_2 \equiv [\text{Mn}_3(\text{CH}_3\text{COO})_6(\text{H}_2\text{O})_4] \cdot 2\text{H}_2\text{O}$ 229
- Figure VI.11** PZC species, $\{\text{Mn}(\text{CH}_3\text{COO})_2(\text{sol})_4\}$ condense to form dimeric unit which extended into the 2D sheet. The overall composition is $\{\text{Mn1}(\text{CH}_3\text{COO})_{4/2}(\text{CH}_3\text{COO}')_{2/3}\}\{\text{Mn2}(\text{CH}_3\text{COO})_{2/2}(\text{CH}_3\text{COO}')_{2/3}(\text{H}_2\text{O})_{2/1}\}_2 \equiv [\text{Mn}_3(\text{CH}_3\text{COO})_6(\text{H}_2\text{O})_4]$ 230
- Figure VI.12** (a) The soluble 1:1 manganese dicarboxylate complex acts as a tecton. (b) Aggregation of these tectons facilitates the formation of a 2D manganese dicarboxylate coordination network through the condensation of carboxylate oxygen with the solvent. (c) The coordinated water interacts with the carboxylate oxygen from the adjacent layer through a strong $\text{O}-\text{H}\cdots\text{O}$ leading to zig-zag sheets. 232
- Figure VI.13** (a) The 1:1 manganese dicarboxylate complex as a tecton. (b) Aggregation of the tectons facilitates the formation of a 2D sheet through the condensation of carboxylate oxygen with the solvent. (c) The weaker $\text{C}-\text{H}\cdots\text{O}$ between DMF and $-\text{COO}$ results in almost parallel layers. 233
- Figure VI.14** (a) The 1:1 manganese dicarboxylate complex acts as a tecton. (b) Aggregation of tectons facilitates the formation of 2D sheets in **3** similar to **2** except for the nature of $\text{C}-\text{H}\cdots\text{O}$ taking place between DMSO and $-\text{COO}$ as shown in (c). 233
- Figure VI.15** Supramolecular condensation of $\{\text{Mn}(4,4'\text{-bpd}c)(\text{phen})(\text{sol})_3\}$ species to facilitate extended metal-ligand coordination linkage forming chains. 235
- Figure VI.16** Supramolecular condensation of the species, $\{\text{Mn}(4,4'\text{-bpd}c)(2,2'\text{-bipy})(\text{sol})_3\}$ and $\{\text{Mn}(4,4'\text{-bpd}c)(\text{sol})_5\}$ in the molar ratio 2:1 leading to a 2D sheet. 236
- Figure VI.17** Supramolecular condensation of the species, $\{\text{Mn}(4,4'\text{-bpd}c)(4,4\text{-dimethyl-}2,2'\text{-bipy})(\text{sol})_3\}$ and $\{\text{Mn}(4,4'\text{-bpd}c)(\text{sol})_5\}$ in the molar ratio 2:1 leading to a 3D structure. 237

Figure VI.18 PZC species, [$\{\text{Mn}(5,5'\text{-dimethyl-}2,2'\text{-bipy})(4,4'\text{-bpd}c)(\text{sol})_3\}\{\{\text{Mn}(5,5'\text{-dimethyl-}2,2'\text{-bipy})(\text{sol})_4\}\{4,4'\text{-bpd}c\}\}$] condense in ratio 1:1 to form one dimensional anionic chain along with cationic complex.....	238
Figure VI.19 Supramolecular condensation of $\{\text{Mn}(4,4'\text{-bpd}c)(4,4'\text{-bipy})(\text{sol})_4\}$ and $\{\text{Mn}(4,4'\text{-bpd}c)(\text{sol})_5\}$ species to facilitate extended metal-ligand coordination linkage forming 2D sheet.....	238
Figure VI.20 Supramolecular condensation of $\{\text{Mn}(2,4'\text{-bpd}c)(\text{sol})_4\}$ species to facilitate extended metal-ligand coordination linkage forming chains.....	240
Figure VI.21 Supramolecular condensation of $\{\text{Mn}(2,4'\text{-bpd}c)(\text{phen})(\text{sol})_3\}$ species leading to 1D chain.....	241
Figure VI.22 Supramolecular condensation of the species, $\{\text{Mn}(2,4'\text{-bpd}c)(\text{sol})_5\}$ and $\{\text{Mn}(2,4'\text{-bpd}c)(2,2'\text{-bipy})(\text{sol})_3\}$ in the molar ratio 1:2 leading to a 2D sheet.....	242
Figure VI.23 Supramolecular condensation of $\{\text{Mn}(2,4'\text{-bpd}c)(4,4'\text{-dimethyl-}2,2'\text{-bipy})(\text{sol})_3\}$ and $\{\text{Mn}(\text{HCOO})_2(\text{sol})_4\}$ species into a 1D chain.....	242
Figure VI.24 Supramolecular condensation of $\{\text{Mn}(2,4'\text{-bpd}c)(4,4'\text{-dimethyl-}2,2'\text{-bipy})(\text{sol})_3\}$ and $\{\text{Mn}(\text{CH}_3\text{COO})_2(\text{sol})_4\}$ leading to a 2D sheet.....	243
Figure VI.25 Supramolecular condensation of $\{\text{Mn}(5,5'\text{-dimethyl-}2,2'\text{-bipy})(2,4'\text{-bpd}c)(\text{sol})_2\}$ and $\{\text{MnCl}_2(\text{sol})_4\}$ species to a 1D chain.....	244
Figure VI.26 Supramolecular condensation of $\{\text{Mn}(\text{bdc})(4,4'\text{-dimethyl-}2,2'\text{-bipy})(\text{sol})_3\}$ and $\{\text{Mn}(\text{bdc})(\text{sol})_5\}$ leading to a 2D sheet.....	246
Figure VI.27 Supramolecular condensation of $\{\text{Mn}(\text{bdc})(4,4'\text{-dimethyl-}2,2'\text{-bipy})(\text{sol})_3\}$ and $\{\text{Mn}(\text{bdc})(\text{sol})_5\}$ leading to a 2D sheet.....	247
Figure VI.28 Supramolecular condensation of $\{\text{Mn}(5,5'\text{-dimethyl-}2,2'\text{-bipy})(\text{bdc})(\text{sol})_3\}$ leading to 1D chains.....	248
Figure VI.29 Supramolecular condensation of $\{\text{Mn}(5,5'\text{-dimethyl-}2,2'\text{-bipy})(\text{nda})(\text{sol})_3\}$ and $\{\text{MnCl}_2(5,5'\text{-dimethyl-}2,2'\text{-bipy})(\text{sol})_2\}$ leading to 1D chains.....	248
Figure VI.30 Supramolecular condensation of $\{\text{MnCl}_2(5,5'\text{-dimethyl-}2,2'\text{-bipy})(\text{sol})_2\}$ and $\{\text{Mn}(\text{nda})(\text{sol})_5\}$ leading to 2D sheets.....	249
Figure VI.31 Supramolecular condensation of $\{\text{Mn}(5,5'\text{-dimethyl-}2,2'\text{-bipy})(\text{nda})(\text{sol})_3\}$ and $\{\text{Mn}(\text{nda})(\text{sol})_5\}$ leading to 3D structure.....	250

LIST OF TABLES

Table I.1. Magnetic behavior of simple manganese (II) salts.....	12
---	----

Table I.2 Structural diversities and magnetic behavior of manganese-semirigid carboxylate-based coordination polymers reported in the literature.....	23
Table II.1 Crystallization of solids from the system Mn(II) salt – 4,4'- <i>H₂bpdc</i> –solvent at 110 °C.....	47
Table II.2 Crystallization of solids from the system Mn(II) salt – 4,4'- <i>H₂bpdc</i> –solvent at 110 °C.....	48
Table II.3 Crystallization of solids from the system Mn(II) salt – 4,4'- <i>H₂bpdc</i> –solvent at 140 °C.....	49
Table II.4 Bond valence sum for MnCP1-MnCP3.....	52
Table II.5 Crystal data and structure refinement details for MnCP1-MnCP3.....	54
Table II.6 Thermogravimetric calculations for solids MnCP1-MnCP3.....	64
Table II.7 Magnetic properties of MnCP1-MnCP3.....	68
Table II.8 Selected bond lengths (Å) and angles (°) for MnCP1-MnCP3.....	72
Table III.1 Crystallization of solids from the system Mn(II) salt –4,4'- <i>H₂bpdc</i> – <i>phen</i> –solvent at 140 °C.....	82
Table III.2 Crystallization of solids from the system Mn(II) salt –4,4'- <i>H₂bpdc</i> –2,2'- <i>bipy</i> –solvent at 110 °C.....	83
Table III.3 Crystallization of solids from the system Mn(II) salt –4,4'- <i>H₂bpdc</i> –4,4'- <i>dimethyl-2,2'-bipy</i> –solvent at 110 °C.....	85
Table III.4 Crystallization of solids from the system Mn(II) salt –4,4'- <i>H₂bpdc</i> –5,5'- <i>dimethyl-2,2'-bipy</i> –solvent at 110 °C.....	87
Table III.5 Crystallization of solids from the system Mn(II) salt –4,4'- <i>H₂bpdc</i> –4,4'- <i>bipy</i> –solvent at 140 °C.....	88
Table III.6 Bond valence sum for MnCP4, MnCP5, MnCP8, MnCP9 and MnCP10.....	92
Table III.7 Crystal data and structure refinement details for solid MnCP4-MnCP10.....	94
Table III.8 Magnetic properties of solids MnCP4-MnCP10.....	112
Table III.9 Selected bond lengths (Å) and angles (°) for MnCP4-MnCP10.....	114

Table IV.1 Crystallization of solids from the system Mn(II) salt – 2,4'- <i>H₂bpdc</i> –solvent at 110 °C.....	123
Table IV.2 Crystallization of solids from the system Mn(II) salt – 2,4'- <i>H₂bpdc</i> – <i>phen</i> –solvent at 110 °C.....	124
Table IV.3 Crystallization of solids from the system Mn(II) salt – 2,4'- <i>H₂bpdc</i> –2,2'- <i>bipy</i> –solvent at 110 °C.....	125
Table IV.4 Crystallization of solids from the system Mn(II) salt – 2,4'- <i>H₂bpdc</i> –4,4'- <i>dimethyl-2,2'-bipy</i> –solvent at 110 °C.....	126
Table IV.5 Crystallization of solids from the system Mn(II) salt – 2,4'- <i>H₂bpdc</i> –5,5'- <i>dimethyl-2,2'-bipy</i> –solvent at 110 °C.....	128
Table IV.6 Bond valence sum for MnCP11-MnCP16.....	132
Table IV.7 Crystal data and structure refinement details for MnCP11-MnCP16.....	135
Table IV.8 Magnetic properties of solids MnCP11-MnCP14 and MnCP16.....	157
Table IV.9 Selected bond lengths (Å) and angles (°) for MnCP11-MnCP16.....	158
Table V.1. Crystallization of solids from the system Mn(II) salt – <i>H₂bdc</i> –4,4'- <i>dimethyl-2,2'-bipy</i> –solvent at 110 °C.....	166
Table V.2 Crystallization of solids from the system Mn(II) salt – <i>H₂bdc</i> –5,5'- <i>dimethyl-2,2'-bipy</i> –solvent at 110 °C.....	167
Table V.3 Crystallization of solids from the system Mn(II) salt – <i>H₂bdc</i> –3,4,7,8- <i>tetramethyl-phen</i> –solvent at 110 °C.....	169
Table V.4 Crystallization of solids from the system Mn(II) salt – <i>H₂bdc</i> –4,4'- <i>dimethyl-2,2'-bipy</i> –solvent at 110 °C.....	170
Table V.5 Crystallization of solids from the system Mn(II) salt – <i>H₂nda</i> –5,5'- <i>dimethyl-2,2'-bipy</i> –solvent at 110 °C.....	172
Table V.6 Crystallization of solids from the system Mn(II) salt – <i>H₂bdc</i> –3,4,7,8- <i>tetramethyl-phen</i> –solvent at 110 °C.....	173
Table V.7 Bond valence sum for MnCP17-MnCP25.....	179
Table V.8 Crystal data and structure refinement details for MnCP17-MnCP25.....	182
Table V.9 Magnetic properties of solids.....	212
Table V.10 Selected bond lengths (Å) and angles (°) for MnCP17-MnCP25.....	212

Table VI.1 Crystallographic data of Mn(II) salts.....	224
--	-----

LIST OF SCHEMES

Scheme II.1 Crystallization of manganese(II) dicarboxylate CPs aggregating from manganese solvated complex and dicarboxylate anion in the given solvent.....	51
Scheme II.2 Coordination modes of Mn(II) in solids MnCP1- MnCP3.....	57
Scheme III.1 Molecular structure of <i>4,4'-H₂bpd</i> c and N-donor auxiliary ligands reported in this chapter.....	81
Scheme III.2 Crystallization of manganese(II) dicarboxylate coordination polymers aggregating from manganese solvated complex and dicarboxylate anion in the given solvent.....	90
Scheme III.3 Coordination environments of Mn(II) in solids MnCP4-MnCP10.....	96
Scheme III.4 Coordination modes of Mn(II) in solids MnCP4–MnCP10.....	97
Scheme IV.1 Molecular structure of the dicarboxylic acid and N-donor auxiliary ligands used in this study.....	121
Scheme IV.2 A schematic representation of the synthetic protocol for solids MnCP11-MnCP16 isolated in the system, manganese chloride-auxiliary ligand- <i>2,4'-bpd</i> c-solvent.....	130
Scheme IV.3 Coordination environments of Mn(II) in solids MnCP11-MnCP16.....	137
Scheme IV.4 Coordination modes of <i>2,4'-bpd</i> c in solids MnCP11–MnCP16.....	138
Scheme V.1 Molecular structure of the dicarboxylic acid and N-donor auxiliary ligands used in this study.....	164
Scheme V.2 Crystallization of manganese(II) dicarboxylate (<i>bdc</i>) coordination polymers aggregating from manganese solvated complex and dicarboxylate anion in the given solvent.....	175
Scheme V.3 Crystallization of manganese(II) dicarboxylate (<i>nda</i>) coordination polymers aggregating from manganese solvated complex and dicarboxylate anion in the given solvent.....	175
Scheme V.4 Coordination environments of Mn(II) in solids MnCP17-MnCP25.....	185
Scheme V.5 Coordination modes of dicarboxylates in solids MnCP17–MnCP25.....	187

Scheme VI.1 A representative example of supramolecular toolbox.....	231
Scheme VI.2 A schematic representation of supramolecular toolbox for the system Mn(II) -4,4'- <i>H₂bpdC</i> -auxiliary ligand-solvent.....	234
Scheme VI.3 A schematic representation of supramolecular toolbox Mn(II) -2,4'- <i>H₂bpdC</i> -auxiliary ligand-solvent.....	239
Scheme VI.4 A schematic representation of supramolecular toolbox manganese(II)- rigid aromatic dicarboxylic acid-auxiliary ligand-solvent.....	245

Abbreviations

1. *4,4'*-*H₂bpdc* = benzophenone-4,4'-dicarboxylic acid
2. *2,4'*-*H₂bpdc* = benzophenone-2,4'-dicarboxylic acid
3. *bdc* = 1, 4-benzenedicarboxylic acid
4. *nda* = Naphthalene-2,6'-dicarboxylic acid
5. *2,2'*-*bipy* = 2,2'-bipyridine
6. *4,4'*-*bipy* = 4,4'-bipyridine
7. *phen* = 1,10 phenanthroline
8. *4,4'*-*dimethyl-2,2'*-*bipy* = 4,4'-dimethyl-2,2'-bipyridine
9. *5,5'*-*dimethyl-2,2'*-*bipy* = 5,5'-dimethyl-2,2'-bipyridine
10. DMF = N, N'-dimethyl formamide
11. DMA = N, N'-dimethyl acetamide
12. DMSO = Dimethyl sulphoxide
13. THF = Tetrahydro furan
14. CH₃CN = Acetonitrile
15. MeOH = Methanol
16. EtOH = Ethanol
17. *H₂SBA* = 4,4'-sulfonyldibenzoic